The η- and η'-Nucleus Interactions and the Search for η, η'- Mesic States

Steven D. Bass, Volker Metag, and Pawel Moskal

Contents

Abstract

The isoscalar η and η' mesons are special in QCD, being linked both to chiral symmetry and to non-perturbative glue associated with the axial anomaly. The properties of these mesons in medium are sensitive to how these dynamics

S. D. Bass
Kitzbühel Centre for Physics, Kitzbühel, Austria
Marian Smoluchowski Institute of Physics and Institute of Theoretical Physics, Jagiellonian University, Kraków, Poland
e-mail: Steven.Bass@cern.ch

V. Metag (✉)
II. Physikalisches Institut, University of Giessen, Giessen, Germany
e-mail: Volker.metag@exp2.physik.uni-giessen.de

P. Moskal
Marian Smoluchowski Institute of Physics and Center for Theranostics, Jagiellonian University, Kraków, Poland
e-mail: p.moskal@uj.edu.pl

I. Tanihata et al. (eds.), *Handbook of Nuclear Physics*,
https://doi.org/10.1007/978-981-15-8818-1_39-1

work in the nuclear environment. In contrast to pionic and kaonic atoms which are mainly bound by the Coulomb interaction with some corrections due to the strong force (Coulomb-assisted binding), the η and η' as neutral mesons can only be bound by the strong interaction. Is this interaction strong enough? This topic has inspired a vigorous program of experiments, conducted in close contact with theory. One has to determine the complex η, η'-nucleus potential. Does the real part V provide a sufficiently deep potential? Is the imaginary part W small enough to allow for narrow states that can more easily be detected experimentally, i.e., $|W| \ll |V|$? The η' effective mass is observed to be suppressed by ≈ -40 MeV at nuclear matter density. Bound state searches are ongoing. This article gives an overview of the status of knowledge in this field together with an outlook to future experiments.

Introduction

Low-energy quantum chromodynamics, QCD, is characterized by confinement and dynamical chiral symmetry breaking. The fundamental quark and gluon degrees of freedom probed in high-energy deep inelastic scattering freeze out into hadrons. One finds nuclei built from protons and neutrons which interact through meson exchanges (pions, ρ, ω, ...) together with an important role for the Δ resonance in low-energy pion nucleon interactions. In the absence of small quark mass contributions, the proton mass is determined by gluonic binding energy. Pions and kaons are would-be Goldstone bosons associated with chiral symmetry with masses squared proportional to the masses of their constituent quarks. Besides the confinement potential, gluonic degrees of freedom are active in the flavor-singlet channel and increase by about 300–400 MeV the masses of their isosinglet partners, the η and η' states, which are then no longer pure Goldstone states.

Hadron properties are modified in nuclear media. Studying these properties using the nucleus as a "detector" opens a new window on low-energy QCD dynamics including chiral symmetry.

One finds a small pion mass shift of order a few MeV in asymmetric nuclear matter (Kienle and Yamazaki 2004). Experiments with deeply bound pionic atoms reveal a reduction in the value of the pion decay constant $f_\pi^{*2}/f_\pi^2 = 0.64 \pm 0.06$ at nuclear matter density (Suzuki et al. 2004). K^--mesons are observed to experience an effective mass drop of the order of 200 MeV at about two times nuclear matter density in heavy-ion collisions (Schroter et al. 1994; Barth et al. 1997). A detailed overview of meson properties in medium is given in Metag et al. (2017). One also finds that the nucleon and Δ masses are suppressed in medium (Oset and Salcedo 1987; Lenske et al. 2018; Lenske and Dhar 2018). What should one expect for the η and η'? How does the gluonic part of their mass behave in nuclei? Can one find η and η' bound states in nuclei? Without its gluonic mass contribution, the η' would be a strange quark state with just small interaction with the light-quark meson mean fields present in the nucleus (Bass and Thomas 2006, 2014).

Meson masses in nuclei are determined from the meson nucleus optical potential and the scalar induced contribution to the meson propagator evaluated at zero three-momentum, $\vec{k} = 0$, in the nuclear medium. Let $k = (E, \vec{k})$ and m denote the four-momentum and mass of the meson in free s pace. Then, one solves the equation

$$k^2 - m^2 = \mathrm{Re}\ \Pi(E, \vec{k}, \rho) \tag{1}$$

for $\vec{k} = 0$ where Π is the in-medium s-wave meson self-energy and ρ is the nuclear density. Contributions to the medium mass come from coupling to the scalar σ field in the nucleus in mean field approximation and to nucleon-hole and resonance-hole excitations in the medium. For $\vec{k} = 0$, $k^2 - m^2 \sim 2m(m^* - m)$ where m^* is the effective mass in the medium. The mass shift $m^* - m$ is the depth or real part of the meson nucleus optical potential. The imaginary part of the potential measures the width of the meson in the nuclear medium.

The s-wave self-energy can be written as (Ericson and Weise 1988; Friedman and Gal 2007)

$$\Pi(E, \vec{k}, \rho)\Big|_{\{\vec{k}=0\}} = -4\pi a\rho\left(1 + \frac{A}{A-1}\frac{\mu}{M}\right) \tag{2}$$

Here a is the meson-nucleon scattering length and ρ is the nuclear density; A is the atomic number, M is the nucleon mass, and $\mu = mM_A/(m + M_A)$ where M_A is the mass of the nucleus. The expression in Eq. (2) is quoted to leading order in a, that is, suppressing higher-order terms in a from Ericson-Ericson-Lorentz-Lorenz multiple scattering corrections.

Attraction corresponds to positive values of a. The meson self-energy is related to the complex meson-nucleus potential $U(r) = V(r) + i \cdot W(r)$ via

$$\begin{aligned} V(r) &= \frac{\mathrm{Re}\ \Pi(E, \vec{k}, \rho(r))}{2 \cdot E} \\ W(r) &= \frac{\mathrm{Im}\ \Pi(E, \vec{k}, \rho(r))}{2 \cdot E} \end{aligned} \tag{3}$$

where r is the distance from the center of the nucleus.

With a strong attractive interaction, there is a chance to form meson bound states in the nuclei (Haider and Liu 1986). If found, these mesic nuclei would be a new state of matter bound just by the strong interaction, without electromagnetic Coulomb effects which are absent for the neutral η and η'. Mesic nuclei differ from mesonic atoms (Yamazaki et al. 1996) where, for example, a π^- is trapped in the Coulomb potential of the nucleus and bound by the electromagnetic interaction (Toki et al. 1989).

For clean observation of a bound state, one needs larger attraction than absorption and thus the real part of the meson-nucleus optical potential to be much bigger than the imaginary part. Does the real part provide a sufficiently deep potential? Is the

imaginary part small enough to allow for narrow states that can more easily be detected experimentally?

Studies involving bound state searches and excitation functions of mesons in photoproduction from nuclear targets give information about the η and η' meson nucleus optical potentials (Metag et al. 2017; Bass and Moskal 2019).

Strong attractive interactions between the η and η' mesons and nucleons mean that both the η and η' are prime targets for mesic nuclei searches, with a vigorous program of experiments (Metag et al. 2017) in Germany and Japan, plus equally vigorous theoretical activity.

For the η, hints for a possible bound state come from a sharp rise in the production cross sections close to threshold in photoproduction experiments from ^{3}He at Mainz (Pfeiffer et al. 2004; Pheron et al. 2012) and in proton-deuteron (pd) and deuteron-deuteron (dd) reactions at COSY (Goslawski et al. 2012; Budzanowski et al. 2009a). The most precise direct searches (so far) come from the WASA@COSY experiment with focus on possible ^{3}He (Adlarson et al. 2020a, b) and ^{4}He η (Adlarson et al. 2017) bound states. While no clear signal is seen within the systematic errors of the experiments, an ^{3}He-η bound state is not excluded and tight constraints obtained on possible bound state production cross sections. Eta bound states in helium require a large $\eta-$nucleon scattering length with real part greater than about 0.7–1.1 fm (Barnea et al. 2017a, b; Fix and Kolesnikov 2017). New studies of the γd reaction at the ELPH laboratory in Japan see an interesting structure in the $M_{\eta d}$ invariant mass distribution close to the ηd threshold which might be evidence for an η two-nucleon bound state or an ηd virtual state due to strong ηd attraction (Ishikawa et al. 2021).

Recent measurements of η' photoproduction from carbon and niobium nuclear targets have been interpreted to imply an effective mass shift ≈ -40 MeV as well as small η' width $\approx$13 MeV in nuclei at nuclear matter density (Nanova et al. 2012, 2013, 2016, 2018; Friedrich et al. 2016) that might give rise to relatively narrow bound η'-nucleus states accessible to experiments. New experimental groups are looking for possible η' bound states in carbon using the (p, d) reaction at GSI/FAIR (Tanaka et al. 2016, 2018; Itahashi et al.), and photoproduction studies at Spring-8 with carbon and copper targets (Shimizu 2017; Tomida et al. 2020).

The plan of this paper is as follows. The section "The η' and η Mesons with Coupling to Anomalous Glue" highlights the special role of the η and η' mesons in low energy QCD. The section "Medium Modifications" then discusses the theory of medium modifications, focusing in the section "Modeling the η' and η in Medium" on theoretical predictions for the η and η' properties in medium. Next, the section "The η -Nucleus Interaction and the Search for η Mesic States" turns to experiments on the η in medium with emphasis on new WASA@COSY results and ongoing experiments in Japan. The section "The η' -Nucleus Interaction and the Search for η' Mesic States" discusses Bonn, GSI, and Spring-8 measurements of the η' in medium and the search for bound states with outlook to new planned experiments at GSI/FAIR. Finally, the section "Conclusions" summarizes the paper with an outlook to future experiments. Complementary reviews of η and η'

interactions with nucleons and nuclei are given in Metag et al. (2017) and Bass and Moskal (2019).

The η' and η Mesons with Coupling to Anomalous Glue

Spontaneous chiral symmetry breaking means that the chiral symmetry of the QCD Lagrangian is broken in the vacuum. One finds a non-vanishing chiral condensate connecting left- and right-handed quarks

$$\langle \text{vac}|\bar{\psi}\psi|\text{vac}\rangle < 0. \tag{4}$$

This spontaneous symmetry breaking induces an octet of light-mass pseudoscalar Goldstone bosons associated with SU(3): the pions and kaons and also (before extra gluonic effects in the singlet channel) an isosinglet Goldstone state.

The Goldstone bosons P couple to the axial-vector currents which play the role of Noether currents through

$$\langle \text{vac}|J^i_{\mu 5}|P(p)\rangle = -if^i_P\ p_\mu e^{-ip.x} \tag{5}$$

with f^i_P the corresponding decay constants (which determine the strength for, e.g., $\pi^- \to \mu^-\bar{\nu}_\mu$) and satisfy the Gell-Mann-Oakes-Renner (GMOR) relation (Gell-Mann et al. 1968)

$$m^2_P f^2_\pi = -m_q \langle \text{vac}|\bar{\psi}\psi|\text{vac}\rangle + \mathcal{O}(m^2_q) \tag{6}$$

with $f_\pi = \sqrt{2}F_\pi = 131$ MeV. The mass squared of the Goldstone bosons m^2_P is in first order proportional to the mass of their valence quarks m_q.

This picture is the starting point of successful pion and kaon phenomenology. The QCD Hamiltonian is linear in the quark masses. For small quark masses, this allows one to perform a rigorous expansion perturbing in $m_q \propto m^2_\pi$, called the chiral expansion (Gasser and Leutwyler 1982). The lightest up and down quark masses are determined from detailed studies of chiral dynamics. One finds $m_u = 2.2^{+0.5}_{-0.3}$ MeV and $m_d = 4.7^{+0.5}_{-0.2}$ MeV, whereas the strange quark mass is slightly heavier at $m_s = 93^{+11}_{-5}$ MeV (with all values here quoted at the scale $\mu = 2$ GeV according to the Particle Data Group (Zyla et al. 2020)).

Whereas Eq. (6) works very well for the flavor non-singlet pions and kaons, the isosinglet η and η' are more subtle due to gluonic effects in the flavor-singlet channel. The quark condensate in Eq. (6) also spontaneously breaks axial U(1) symmetry meaning that one might also expect a flavor-singlet Goldstone state which mixes with the octet state to generate the isosinglet bosons. However, without extra input, the resultant bosons do not correspond to states in the physical spectrum. The lightest mass isosinglet bosons, the η and η', with masses $m_\eta = 548$ MeV and $m_{\eta'} = 958$ MeV are about 300–400 MeV too heavy to be pure Goldstone states.

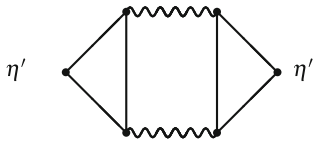

Fig. 1 Gluonic intermediate states contribute to the η'. The η' mixes a chirality-two quark-antiquark contribution and chirality-zero gluonic contribution

The extra ingredient is a gluonic mass term in the flavor-singlet channel. In the singlet channel, the quark-antiquark pair (with quark chirality equal two) propagates with coupling to non-perturbative gluonic intermediate states (with zero net chirality); see Fig. 1.

To see the effect of this gluonic mass contribution, consider the η-η' mass matrix for free mesons with rows and columns in the octet-singlet basis $\eta_8 = \frac{1}{\sqrt{6}}\,(u\bar{u} + d\bar{d} - 2s\bar{s})$ and $\eta_0 = \frac{1}{\sqrt{3}}\,(u\bar{u} + d\bar{d} + s\bar{s})$. Expressing these in terms of the pion and kaon mass squared, at leading order in the chiral expansion (taking terms proportional to the quark masses m_q), this reads

$$M^2 = \begin{pmatrix} \frac{4}{3}m_{\rm K}^2 - \frac{1}{3}m_\pi^2 & -\frac{2}{3}\sqrt{2}(m_{\rm K}^2 - m_\pi^2) \\ -\frac{2}{3}\sqrt{2}(m_{\rm K}^2 - m_\pi^2) & [\frac{2}{3}m_{\rm K}^2 + \frac{1}{3}m_\pi^2 + \tilde{m}_{\eta_0}^2] \end{pmatrix}. \tag{7}$$

Here $\tilde{m}_{\eta_0}^2$ is the flavor-singlet gluonic mass term.

The masses of the physical η and η' mesons are found by diagonalizing this matrix, *viz.*

$$\begin{aligned} |\eta\rangle &= \cos\theta\ |\eta_8\rangle - \sin\theta\ |\eta_0\rangle \\ |\eta'\rangle &= \sin\theta\ |\eta_8\rangle + \cos\theta\ |\eta_0\rangle \end{aligned} \tag{8}$$

One obtains values for the η and η' masses:

$$m_{\eta',\eta}^2 = (m_{\rm K}^2 + \tilde{m}_{\eta_0}^2/2) \pm \frac{1}{2}\sqrt{(2m_{\rm K}^2 - 2m_\pi^2 - \frac{1}{3}\tilde{m}_{\eta_0}^2)^2 + \frac{8}{9}\tilde{m}_{\eta_0}^4}. \tag{9}$$

Here the lightest mass state is the η and heavier state is the η'. Summing over the two eigenvalues in Eq.(9) gives the Witten-Veneziano mass formula (Witten 1979; Veneziano 1979)

$$m_\eta^2 + m_{\eta'}^2 = 2m_K^2 + \tilde{m}_{\eta_0}^2. \tag{10}$$

The gluonic mass term is obtained by substituting the physical values of m_η, $m_{\eta'}$ and m_K to give $\tilde{m}_{\eta_0}^2 = 0.73\,\text{GeV}^2$. In QCD, $\tilde{m}_{\eta_0}^2$ is related to a quantity called the Yang-Mills topological susceptibility. Its value is induced by non-perturbative

gluon dynamics and topological structure in QCD vacuum associated with the QCD axial anomaly (Shore 2008) , e.g., instantons and perhaps gluon dynamics related to confinement.

In recent computational QCD lattice calculations (Cichy et al. 2015), the gluonic term on the right-hand side of Eq. (10) and the meson mass contributions (with dynamical quarks) were both computed. These calculations verified the Witten-Veneziano mass formula at the 10% percent level in the QCD lattice approach.

Without the gluonic mass term, the η would be approximately an isosinglet light-quark state ($\frac{1}{\sqrt{2}}|\bar{u}u + \bar{d}d\rangle$) with mass $m_\eta \sim m_\pi$ degenerate with the pion and the η' would be a strange-quark state $|\bar{s}s\rangle$ with mass $m_{\eta'} \sim \sqrt{2m_{\rm K}^2 - m_\pi^2}$ — mirroring the isoscalar vector ω and ϕ mesons.

When interpreted in terms of the leading order mixing scheme, Eq. (8), phenomenological studies of various decay processes give a value for the η-η' mixing angle between $-15°$ and $-20°$ (Gilman and Kauffman 1987; Ball et al. 1996; Ambrosino et al. 2009). The η' has a large flavor-singlet component with strong affinity to couple to gluonic degrees of freedom.

In the octet channel, the leading order mass term in Eq. (7) before mixing with the singlet state is the Gell-Mann Okudo mass term $m_{\eta_8}^2 = \frac{1}{3}(4m_K^2 - m_\pi^2)$. Numerically, m_{η_8} agrees with the η meson mass to within 4%. However, large mixing through the strange quark mass means that non-perturbative glue through axial U(1) dynamics plays an important role with both the η and η' and their interactions. The role of singlet degrees of freedom in the η may be essential to understanding the η-nucleon scattering length $a_{\eta N}$; see the section "Modeling the η' and η in Medium".

Besides the meson masses, gluonic degrees of freedom are important in axial U(1) dynamics, and their effect can be included in an extended effective chiral Lagrangian for low-energy QCD (Di Vecchia and Veneziano 1980; Witten 1980). Applications include gluonic contributions to the η'-nucleon coupling constant (Bass 1999), the proton's flavor-singlet axial-charge (Shore and Veneziano 1992) which is related to quark spin content of the proton (Bass 2005; Aidala et al. 2013), and resonant behavior in $\eta'\pi$ re-scattering which yields a possible interpretation of the lightest mass 1^{-+} exotic state found with mass in the range 1400–1600 MeV (Bass and Marco 2002), as well as $\eta \to 3\pi$ decays (Leutwyler 2013).

So far, the η and η' have been discussed at leading order in the chiral expansion. Going beyond leading order, one becomes sensitive to extra SU(3) breaking through the difference in the pion and kaon decay constants, $F_K = 1.22 F_\pi$, as well as new gluonic mediated couplings. One finds strong mixing also in the decay constants. Two mixing angles enter the $\eta - \eta'$ system when one extends the theory to $\mathcal{O}(p^4)$ in the meson momentum (Leutwyler 1998; Feldmann et al. 1999).

There are several places that glue enters η' and η meson physics: the gluon topology potential which generates the large η' and η masses, possible small mixing with a lightest mass pseudoscalar glueball state (which comes with a kinetic energy term in its Lagrangian), and, in high momentum transfer processes, radiatively generated glue associated with perturbative QCD. Possible candidates for the pseudoscalar glueball state are predicted by lattice QCD calculations with a mass

above 2 GeV (Morningstar and Peardon 1999; Gregory et al. 2012). These different gluonic contributions are distinct physics.

Medium Modifications

Hadron properties change in medium. As mentioned in the section "Introduction", the pion decay constant which acts as an order parameter for chiral symmetry is suppressed in medium. Hadron masses and widths are also density (and temperature) dependent. The study of the QCD phase diagram is one of the main topics in QCD research (McLerran 2020; Braun-Munzinger and Wambach 2009) with implications for neutron star structure and the QCD phase transition in the (very hot) early Universe.

This article focuses on hadrons at finite nuclear density and zero temperature. In medium, key issues are the effect of the scalar σ (correlated two-pion exchange) mean field as well as ρ and ω mean fields in the nucleus (Saito et al. 2007), as well as explicit pion cloud and rescattering effects in the nuclear medium (Ericson and Weise 1988).

Medium modifications are observed from low energy properties (Metag et al. 2017) to deep inelastic scattering from nuclear targets, which reveals that the quark momentum distributions in the proton are modified when the proton is in a nuclear environment (Aubert et al. 1983; Cloët et al. 2019).

In Gamow-Teller transitions, the proton's isovector axial-charge $g_A^{(3)}$ is observed to be quenched by about 20% in large nuclei (Ericson and Weise 1988; Suhonen 2018). Theoretically, this follows from pion cloud effects in the nucleus as well as Ericson-Ericson-Lorentz-Lorenz rescattering corrections (Ericson 1998; Ericson et al. 1973). Through the Bjorken sum-rule (Bjorken 1966, 1970), this quenching of $g_A^{(3)}$ also means that the protons' internal spin structure probed in polarized deep inelastic scattering is expected to be modified in medium (Bass 2021), a result found also in partonic models (de Barbaro et al.; Guzey and Strikman 2000; Sobczyk and Szwed 2001; Cloet et al. 2005). Medium dependence of nucleon spin structure should persist also to polarized photoproduction on polarized nucleons in nuclear targets. The Gerasimov-Drell-Hearn sum-rule (Gerasimov 1966; Drell and Hearn 1966) relates the difference in the two spin cross sections to the ratio of anomalous magnetic moment and nucleon's mass all squared, with both of these terms expected to be medium dependent (Bass 2021).

In the medium, besides changes in pion and kaon masses, the anti-proton effective mass is observed to be reduced by about 100–150 MeV below their mass in free space at 2 times nuclear matter density (Schroter et al. 1994). Reduction of the nucleon and Δ masses by about -30 MeV has been discussed in Oset and Salcedo (1987). In recent measurements, the Δ effective mass was observed to be shifted by about -60 MeV in peripheral and central heavy-ion collisions (Lenske et al. 2018; Lenske and Dhar 2018). In contrast, the effective mass of the N*(1535) nucleon resonance which couples strongly to the η meson is observed

to be approximately density independent in heavy-ion collisions (Averbeck et al. 1997) and photoproduction experiments (Röbig-Landau et al. 1996; Yorita et al. 2000), though some evidence for broadening was observed (Yorita et al. 2000).

What should one expect for the η and η' in medium? As explained in the section "Modeling the η' and η in Medium", their masses are expected to be medium dependent with the chance for bound states in light nuclei.

In addition to finite density, more generally in the QCD phase diagram, axial U(1) symmetry is also expected to be (partially) restored at finite temperature (Kapusta et al. 1996). This finite temperature result is observed in recent QCD lattice calculations (Bazavov et al. 2012; Tomiya et al. 2017; Aoki et al. 2021).

Modeling the η' and η in Medium

The η and η' in medium have been addressed in the context of the mean field quark-meson coupling model, QMC (Bass and Thomas 2006, 2014), as well as chiral coupled channels (Nagahiro et al. 2012), Nambu-Jona-Lasinio (Nagahiro et al. 2006; Bernard and Meißner 1988), and linear σ model (Sakai and Jido 2013) calculations.

This section focuses on the QMC approach, which predicts an η' effective mass shift of ≈ -37 MeV at nuclear matter density ρ_0, the one model prediction very similar to the results of the CBELSA/TAPS experiment discussed in the section "The η'-Nucleus Interaction and the Search for η' Mesic States" below (Bass and Thomas 2006, 2014). In the QMC model medium, modifications are calculated at the quark level through coupling of the light quarks in the hadron to the scalar isoscalar σ (and also ω and ρ) mean fields in the nucleus (Saito et al. 2007; Guichon 1988; Guichon et al. 1996). One works in mean field approximation. The couplings of light-quarks to the σ (and ω and ρ) mean fields in the nucleus are adjusted to fit the saturation energy and density of symmetric nuclear matter and the bulk symmetry energy.

The large η and η' masses are used to motivate taking a MIT bag description for the meson wavefunctions, (Tsushima et al. 1998; Tsushima 2000). Phenomenologically, the MIT bag gives a good fit to meson properties in free space for the kaons and heavier hadrons (DeGrand et al. 1975). Gluonic topological effects are understood to be "frozen in," meaning that they are only present implicitly through the masses and mixing angle in the model. The strange-quark component of the wavefunction does not couple to the σ mean field, and η-η' mixing is readily built into the model. Possible binding energies and the in-medium masses of the η and η' are sensitive to the flavor-singlet component in the mesons and hence to the non-perturbative glue associated with axial U(1) dynamics (Bass and Thomas 2006). Working with the mixing scheme in Eq. (8) with an η-η' mixing angle of $-20°$, the QMC prediction for the η' mass in medium at nuclear matter density is 921 MeV, that is a mass shift of -37 MeV. This value is in excellent agreement with the mass shift $-40 \pm 6 \pm 15$ MeV deduced from photoproduction data; see Eq. (18) in the section "The η'-Nucleus Interaction and the Search for η' Mesic States". Mixing increases the octet relative to singlet component in the η', reducing the binding

through increased strange quark component in the η' wavefunction. Without the gluonic mass contribution, the η' would be a strange quark state after η-η' mixing. Within the QMC model, there would be no coupling to the σ mean field and no mass shift so that any observed mass shift is induced by non-perturbative glue that generates part of the η' mass.

For the η meson, the potential depth predicted by QMC is ≈ -100 MeV at nuclear matter density with $-20°$ mixing. For a pure octet η, the model predicts a mass shift of ≈ -50 MeV. Increasing the flavor-singlet component in the η at the expense of the octet component gives more attraction, more binding, and a larger value of the η-nucleon scattering length, $a_{\eta N}$.

The mass shifts obtained in the QMC model with mixing angle $-20°$ correspond to meson-nucleon scattering lengths with real parts Re $a_{\eta N} \approx 0.85$ fm and Re $a_{\eta' N} \approx 0.47$ fm. These values are quoted in linear density approximation with the Ericson-Ericson-Lorentz-Lorenz denominator switched off (corresponding to the model mean field approximation). The QMC model makes no statement about the imaginary parts of the meson-nucleus potentials and the corresponding scattering lengths.

In QMC, η-η' mixing with the phenomenological mixing angle $-20°$ leads to a factor of two increase in the mass-shift and in the scattering length obtained in the model relative to the prediction for a pure octet η_8 (Bass and Thomas 2006). This result may explain why values of $a_{\eta N}$ extracted from phenomenological fits to experimental data where the η-η' mixing angle is unconstrained give larger values (with real part about 0.9 fm) than those predicted in theoretical coupled-channel models where the η is treated as a pure octet state.

The QMC model results for the η and η' mass shifts with mixing angle $-20°$ and for nuclear densities ρ between about 0.5 and 1 times ρ_0 are (Bass and Thomas 2006)

$$m^*_\eta/m_\eta \approx 1 - -0.17\ \rho/\rho_0 \qquad (11)$$
$$m^*_{\eta'}/m_{\eta'} \approx 1 - -0.05\ \rho/\rho_0.$$

More generally, within the U(1) extended effective chiral Lagrangian approach, one can couple the gluonic degrees of freedom associated with the square of the topological charge density that gives the large value of $\tilde{m}^2_{\eta_0}$ to the σ mean field in the nucleus. This yields a reduced value for $\tilde{m}^2_{\eta_0}$ independent of the sign of the coupling (Bass and Thomas 2006). In the QMC approach, if one assumes that the mass formula Eq. (7) holds also in symmetric nuclear matter at finite density and substitute the QMC predictions for the η', η kaon masses in medium ($m^*_K = 430.4$ MeV), then one obtains $\tilde{m}^2_{\eta_0} = 0.68\,\text{GeV}^2 < 0.73\,\text{GeV}^2$ at ρ_0 with $\eta - \eta'$ mixing angle equal to $-20°$.

Recent coupled-channel model calculations have appeared with mixing and vector meson channels included, with predictions for η' bound states for a range of possible values of $a_{\eta' N}$ (Nagahiro et al. 2012). Larger mass shifts, downwards by up to 80–150 MeV, were found in Nambu-Jona-Lasinio model calculations (without

confinement) (Nagahiro et al. 2006) and in linear sigma model calculations (in a hadronic basis) (Sakai and Jido 2013) which also gave a rising η effective mass at finite density. An early calculation (Bernard and Meißner 1988) gave close to zero effect for the η'.

For the η'-nucleon scattering length, at tree level the flavor-singlet version of the Weinberg-Tomozawa term has $a_{\eta' N}$ proportional to the meson mass squared, which does not vanish in the chiral limit due to the gluonic contribution $\tilde{m}^2_{\eta_0}$ to the η' mass squared (Bass and Moskal 2019; Bass and Thomas 2010). To this level, one finds a finite value for the real part of $a_{\eta' N}$. This situation contrasts with the isovector scattering length $a_{\pi N}$ where the pion mass squared vanishes with zero quark masses.

For possible η bound states in the nuclei, there are a host of predictions. Experiments have so far focused on light helium nuclei, with the status discussed in detail in the section "The η -Nucleus Interaction and the Search for η Mesic States". Predictions for heavier nuclei are given in Tsushima et al. (1998), Tsushima (2000), Garcia-Recio et al. (2002), Friedman et al. (2013), and Cieplý et al. (2014).

In the following sections, these theoretical considerations are confronted with experimental observations.

The η -Nucleus Interaction and the Search for η Mesic States

While the interaction of pions and kaons with nucleons and nuclei can be studied experimentally using beams of these mesons, η and η' mesons with lifetimes $\leq 10^{-19}$ s are too short-lived to produce particle beams. Information on the η, η' interaction with nucleons and nuclei can thus only be deduced from final state interactions in the production of these mesons off nucleons and nuclei. As pointed out in the Introduction, the meson-nucleus potential can be determined from measurements of the meson-nucleon scattering length, the mass shift, and the absorption of these mesons in the nuclear medium, as well as by the measurements of the energies and widths of the meson-nucleus bound states.

The interaction of η' with nucleons and nuclei will be discussed in the next section. Here the focus is on the η-nucleon interaction that was studied based on the energy dependence of the near-threshold photo- and hadro-production of η meson off nucleons and nuclei.

As explained in the Introduction, the η-nucleon complex optical potential is related to the width and binding energy of the η-nucleus bound state referred to as η mesic nucleus. Based on theoretical estimations that the η-nucleon potential is attractive (Bhalerao and Liu 1985), Haider and Liu (1986) postulated the existence of η-mesic nuclei. This inspired much experimental work though early experimental searches for such states (using photon (Pheron et al. 2012; Baskov et al. 2012), pion (Chrien et al. 1988), proton (Adlarson et al. 2020a, b; Budzanowski et al. 2009b) or deuteron (Adlarson et al. 2013, 2017; Afanasiev et al. 2011; Moskal and Smyrski 2010) beams) was not successful and only upper limits for the production

of η-mesic nuclei, and hence only limits on possible values of the η-nucleon potential parameters have been determined.

Among these early experiments, the COSY-GEM Collaboration (Budzanowski et al. 2009b) studied the reaction p ^{27}Al $\rightarrow ^3$ He $p\pi^-$X at recoil free kinematics. If an η meson were produced here, it would be almost at rest in the laboratory system with chance to be bound. The disintegration of the η mesic state may then occur via the excitation of a N*(1535) resonance decaying into a back-to-back π^-p pair. Some enhancement was observed, though this could also be associated with an excited ^{25}Mg intermediate state. An upper bound for the bound state production cross section of about 0.5 nb was deduced.

The most resent high statistics experiments performed by the WASA-at-COSY collaboration (Adlarson et al. 2013, 2017, 2020a, b) aimed at the observation of the ^{4}He-η and ^{3}He-η mesic nuclei. These experiments were motivated by hints of a strong ^{4}He-η and even stronger ^{3}He-η interaction indicated by the steep growth of the cross sections at the thresholds for the dd $\rightarrow ^4$ Heη (Budzanowski et al. 2009a; Wronska et al. 2005; Willis et al. 1997; Frascaria et al. 1994), γ ^{3}He $\rightarrow ^3$ He η and pd $\rightarrow ^3$ Heη reactions. Figure 2 presents cross-sectional excitation functions for the case of ^{3}He-η. The steep rise of the cross sections observed for both photo- and hadro-production reactions indicates that the effect is due to the He-η final state interaction rather than the initial state reaction dynamics.

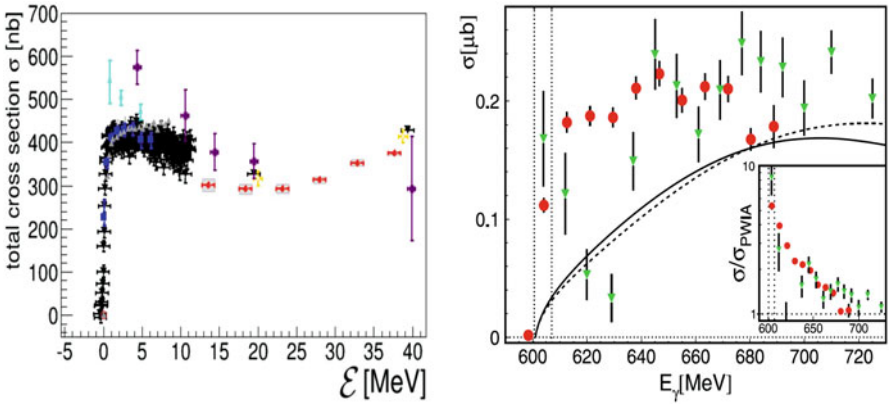

Fig. 2 (Left) Total cross section for the pd $\rightarrow$ ^{3}He η reaction as a function of the excitation energy. Symbols represent experimental results described in Berger et al. (1988), Mayer et al. (1996), Betigeri et al. (2000), Bilger et al. (2002), Smyrski et al. (2007), Adam et al. (2007), Mersmann et al. (2007), Rausmann et al. (2009), and Adlarson et al. (2014, 2018). The sharp rise of the cross section is visible in the short range of about 2 MeV above the reaction threshold. (The figure is taken from Bass and Moskal 2019) (Right) Total cross section for the γ ^{3}He$\rightarrow$ η^3He reaction is shown as a function of the excess energy (Pheron et al. 2012; Pfeiffer et al. 2004). Solid (dashed) Superimposed curves indicate results obtained based on the plane wave impulse approximation (PWIA) calculations with a realistic (solid) and isotropic (dashed) angular distribution for the γn $\rightarrow$ nη reaction. Insert: ratio of measured and PWIA cross sections. (The figure is taken from Pheron et al. 2012)

This conclusion was strengthened by a small and energy-independent value of the analyzing power (Papenbrock et al. 2014) as well as strong variation with energy of the phase of the s-wave production amplitude (Smyrski et al. 2007; Mersmann et al. 2007; Wilkin et al. 2007) as expected for a bound or virtual $^3\mathrm{He} - \eta$ state (Wilkin et al. 2007). Based on the above discussed experimental hints, the WASA-at-COSY experimental searches have focused on possible η bound states in ^{3}He and ^{4}He (Adlarson et al. 2013, 2017, 2020a, b). Also theoretically the existence of the η bound states in helium is predicted, provided that the real part of the $\eta-$nucleon scattering length is greater than about 0.7–1.1 fm (Barnea et al. 2017a, b; Fix and Kolesnikov 2017). This requirement overlaps with the range of values from 0.18 fm (Liu and Zhu 2007) up to 1.07 fm (Green and Wycech 1997) predicted for the real part of the η-nucleon scattering length. The relatively large range of predicted values is due to the different analysis methods. The smallest values, in the order of 0.2 fm, result from chiral coupled channel models where the η meson is treated in pure octet approximation. Moreover, for most of the coupled channel analyses, the imaginary part is larger than the real one (e.g., $a_{\eta\mathrm{N}}$ =0.18+i0.42 fm (Liu and Zhu 2007)), which would imply that the η-mesic nucleus cannot exist. On the other hand, analysis of the experimental data ($\pi\mathrm{N} \rightarrow \pi\mathrm{N}$, $\pi\mathrm{N} \rightarrow \eta\mathrm{N}$, $\gamma\mathrm{N} \rightarrow \pi\mathrm{N}$, $\gamma\mathrm{N} \rightarrow \eta\mathrm{N}$) in the frame of coupled ηN, πN, γN systems, described by a K-matrix, results in scattering lengths even as large as $a_{\eta\mathrm{N}}$ =1.07 fm + i0.26 fm with imaginary part much less than the real one (Green and Wycech 1997) indicating favorable conditions for the creation of the η-mesic nucleus. Compilations of values derived for the η-nucleon scattering length in different approaches may be found in references Sibirtsev et al. (2002) and Arndt et al. (2005).

The key physical process of the η-mesic helium involves a virtual η meson production forming a bound state with the helium nucleus in which it is produced. The process is illustrated in Fig. 3 for the example of the proton-deuteron reaction. The WASA-at-COSY experiment tested two possible decay mechanisms of the η mesic helium. In the first scenario (as shown in Fig. 3), the η meson is absorbed by the nucleon exciting it to the N*(1535) resonance. Subsequently, the N^* decays into a pion-nucleon pair leading to the disintegration of the mesic-nucleus. For this decay mechanism, three reactions were studied: $\mathrm{dd} \rightarrow (^4\mathrm{He}-\eta)_{\mathrm{bound}} \rightarrow ^3\mathrm{He\,p}\,\pi^-$ (Adlarson et al. 2013), $\mathrm{dd} \rightarrow (^4\mathrm{He} - \eta)_{\mathrm{bound}} \rightarrow ^3\mathrm{He\,n}\,\pi^0 \rightarrow ^3\mathrm{He\,n}\,\gamma\gamma$ (Adlarson et al. 2017), and $\mathrm{pd} \rightarrow (^3\mathrm{He} - \eta)_{\mathrm{bound}} \rightarrow \mathrm{dp}\pi^0 \rightarrow \mathrm{d\,p}\,\gamma\gamma$ (Adlarson et al. 2020b). The latter process is shown in Fig. 3. In the second considered mechanism, the virtual η meson is decaying directly, leaving the remaining helium nucleus intact. To test this mechanisms, the $\mathrm{pd} \rightarrow (^3\mathrm{He} - \eta)_{\mathrm{bound}} \rightarrow ^3\mathrm{He}\,3\pi^0 \rightarrow ^3\mathrm{He}\,6\gamma$ and $\mathrm{pd} \rightarrow (^3\mathrm{He} - \eta)_{\mathrm{bound}} \rightarrow ^3\mathrm{He}\,2\gamma$ reaction chains were studied (Adlarson et al. 2020a). In the case of the decay process proceeding via creation of the N*, due to the finite geometrical acceptance of the WASA-at-COSY detector (Adam et al.), the determination of the cross section for the studied reactions required the knowledge of the momentum distribution of the N* resonance inside the mesic-nucleus, and in the case of the second considered mechanism, the knowledge about the Fermi momentum distribution for a bound η meson orbiting around the ^{3}He nucleus is

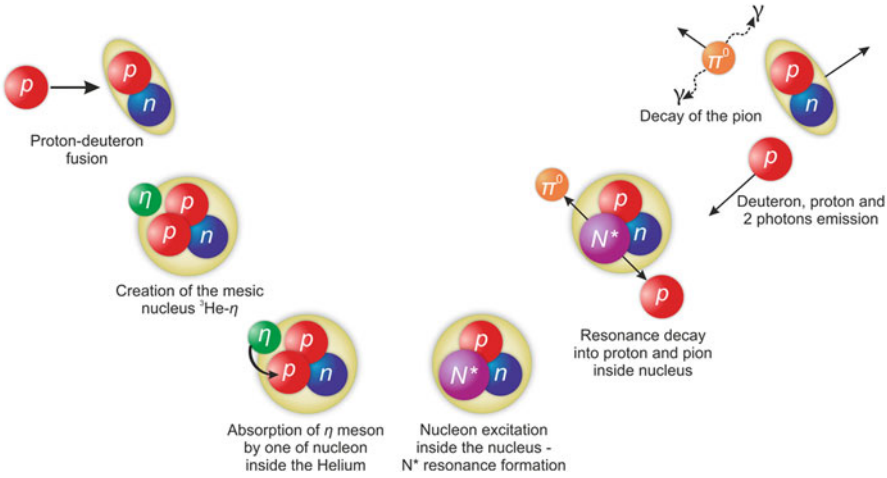

Fig. 3 Sequence of processes leading to the ^{3}He-η bound state production and decay in the pd $\rightarrow$ dpπ^0 reaction. (The figure is taken from Adlarson et al. 2020b)

required. The latter was estimated for various combinations of the ^{3}He-η optical potential parameters in Skurzok et al. (2020). Figure 4 presents the N* momentum distribution in the N*-^{3}He and N*NN systems as estimated recently in Kelkar (2016) and Kelkar et al. (2019, 2020). These distributions were obtained based on the elementary NN* $\rightarrow$ NN* amplitudes within a pion plus η meson exchange model. In Fig. 4, the N*-^{3}He and N*-d momentum distributions are presented for the two chosen binding energies as it is indicated in the legend. The separation energy of nucleons in ^{4}He and ^{3}He is much larger than the binding energy of N*; therefore, the N* momentum distribution is narrower with respect to the distribution of nucleons in helium, as it is visible in Fig. 4. As the result of the performed experiments and the data analysis, the excitation functions around the η meson production thresholds were established for the dd $\rightarrow {}^3$He p π^- Adlarson et al. (2013), dd $\rightarrow {}^3$He n π^0 Adlarson et al. (2017), pd $\rightarrow$ d p π^0 $\rightarrow$ d p $\gamma\gamma$ (Adlarson et al. 2020b), and pd $\rightarrow {}^3$He 2γ and pd $\rightarrow {}^3$He 6γ (Adlarson et al. 2020a). If the production cross section for the creation of the η-helium bound state was larger than the achieved experimental uncertainty, then the bound state would manifest itself as a resonance structure on the excitation function, below the η meson production threshold. Yet, all determined excitation functions were smooth within the error bars and have not revealed any structure which could have been assigned to the formation of η-mesic helium (Adlarson et al. 2013, 2017, 2020a, b). The upper limits of the cross sections for the production and decay of η-mesic ^{4}He and η-mesic ^{3}He are presented in Figs. 5 and 6, respectively.

The achieved experimental sensitivity, $\sim$6 nb for the dd $\rightarrow$ $(^4\mathrm{He} - \eta)_{\mathrm{bound}} \rightarrow {}^3$He p π^- process, and $\sim$3 nb for the dd $\rightarrow$ $(^4\mathrm{He} - \eta)_{\mathrm{bound}} \rightarrow {}^3$He n π^0 process, is at the level of the cross-sectional values expected based on the hypothesis that the

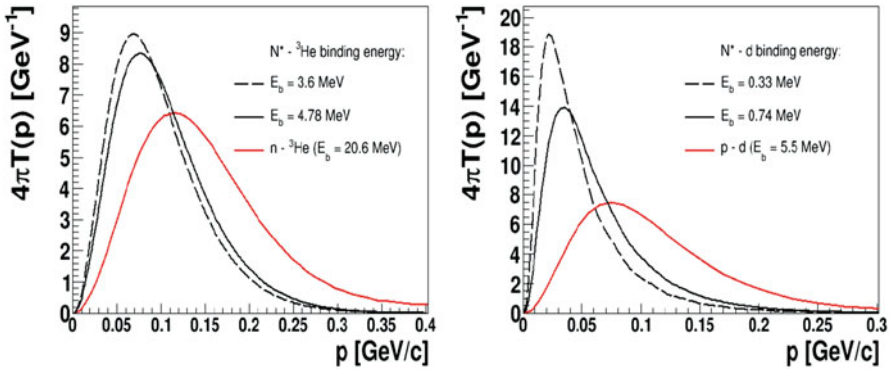

Fig. 4 (Left) Momentum distribution of nucleons and N* inside a ^{4}He calculated assuming N*-^{3}He binding energies of 3.6 and 4.78 MeV, and a n-^{3}He separation energy of 20.6 MeV. (Right) Momentum distribution of the N* and nucleons inside a ^{3}He calculated assuming N*-d binding energies of 0.74 and 0.33 MeV, and a p-^{3}He potential giving proton separation energy of 5.5 MeV (red solid line). (The figures are obtained based on Kelkar (2016), Kelkar et al. (2019, 2020) and are taken from Skurzok (2021). With kind permission of Springer)

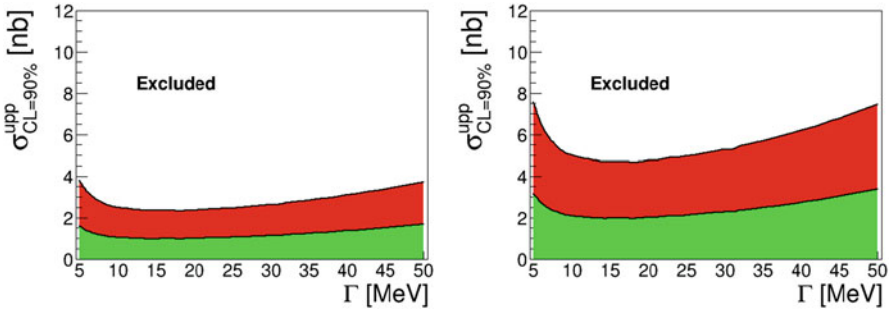

Fig. 5 Upper limit of the total cross section shown as a function of the width of the bound state for the dd $\rightarrow$ (^{4}He-η)$_{\text{bound}}$ $\rightarrow$ ^{3}He$n\pi^0$ (left panel) and the dd $\rightarrow$ (^{4}He-η)$_{\text{bound}}$ $\rightarrow$ ^{3}He$p\pi^-$ (right panel). The values were obtained for the binding energy equal to 30 MeV. The result was determined via the simultaneous fit for both channels. The green area denotes the systematic uncertainties. (The figures are taken from Adlarson et al. 2017)

total cross section of the production of virtual η meson just below the threshold is equal to the cross section of the production of the real η meson above the threshold, which is about 15 nb for the dd $\rightarrow$^{4}He η (Budzanowski et al. 2009a; Wronska et al. 2005; Willis et al. 1997; Frascaria et al. 1994). In the dd $\rightarrow$ (^{4}He $-$ η)$_{\text{bound}}$ $\rightarrow$ ^{3}He p π^- reaction, the more quantitative estimation of the cross section based on the approximation of the scattering amplitude for two body processes results in the value of 4.5 nb (Wycech and Krzemien 2014). A much higher relative precision was achieved in the most recent high statistics search for the ^{3}He-η bound state where the limit of about $\sim$15 nb for the pd $\rightarrow$ (^{3}He $-$ η)$_{\text{bound}}$ $\rightarrow$ dpπ^0 $\rightarrow$ dp $\gamma\gamma$ process (see right panel of Fig. 6) is more than an order of magnitude lower than the close-

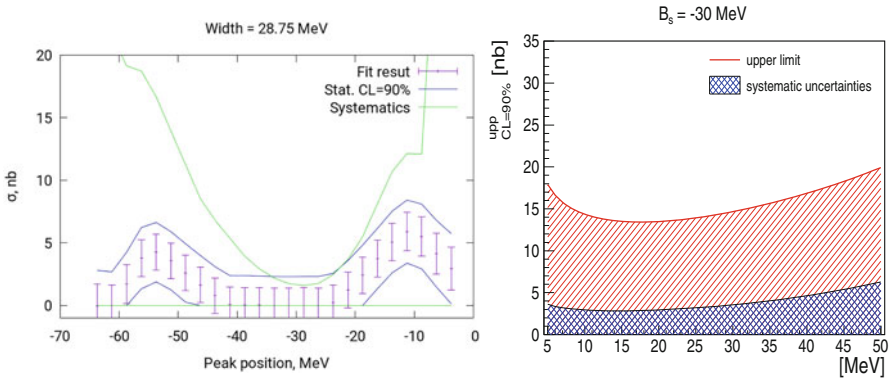

Fig. 6 (Left) Upper limits for cross section of the reaction chain pd $\rightarrow$ (^{3}He-η)$_{\text{bound}}$ $\rightarrow$ ^{3}He(η decays) as function of the binding energy, assuming in the analysis the width Γ=28.75 MeV. The blue and green lines show the range of possible bound state production cross section including statistical and systematic uncertainty, respectively. (The figure is taken from Adlarson et al. 2020a) (Right) The upper limit (90% CL) of the total cross section for formation of the ^{3}He-η bound state and its decay via the $pd \rightarrow$ (^{3}He-η)$_{\text{bound}}$ $\rightarrow$ dpπ^0 reaction as a function of the width of the bound state. The result for the binding energy of $B_s = -30$ MeV is shown. The blue checkered area at the bottom represents the systematic uncertainties. (The figure is taken from Adlarson et al. 2020b)

to-threshold total cross section for creation of the real η meson in the pd $\rightarrow$ ^{3}He η process, which is about 400 nb (see Fig. 2).

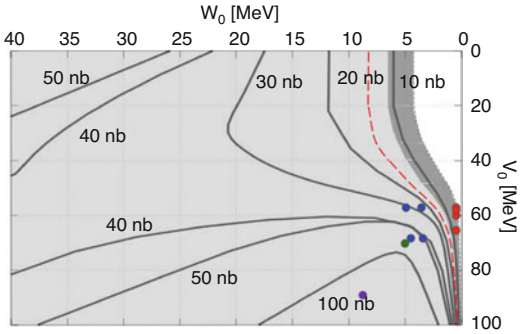

Fig. 7 Contour plot in V_0-W_0 plane of the cross section for the η-mesic ^{4}He production in dd reactions. The red curve separates the allowed parameter region (on the right) from the excluded region determined based on the experimental limits of the cross sections. Dots correspond to the optical potential parameters of the predicted η-mesic ^{4}He states (see text for details). (The figure is taken from Skurzok et al. (2018))

First quantitative estimations of the η-mesic ^{4}He production cross section as a function of the complex optical potential parameters (V_0, W_0) were presented in Ikeno et al. (2017). In the model of Ikeno et al. (2017), the Green's function

technique is used to sum up all η-^{4}He final states for the estimation of the fusion and η meson production processes. The results compared to the experimentally determined excitation functions resulted in the determination of the exclusion region of (V_0, W_0) parameters (Skurzok 2021; Skurzok et al. 2018) which is presented in Fig. 7. The parameters resulting in a cross section larger than 10.7 nb (dark shaded are include systematic errors) were excluded at the 90% CL (Skurzok et al. 2018). The figure indicates that most of the model parameter space is excluded, except for the values of the real and imaginary parts of the potential where V_0 is in the range ~ -60 MeV to 0 and W_0 is between ~ -7 MeV and 0 (Skurzok et al. 2018). Purple and green dots in the excluded region denote predictions based on the few body formalism with an optical model (Barnea et al. 2017b) where the complex η-nucleon scattering amplitude is obtained (i) from a K-matrix description of the πN, $\pi\pi$N, ηN, and γN coupled channels and fit to existing data (purple dot) (Green and Wycech 2005) and (ii) a chirally motivated separable potential model with the parameters fitted to $\pi\mathrm{N} \rightarrow \pi\mathrm{N}$ and $\pi\mathrm{N} \rightarrow \eta\mathrm{N}$ data (green dot) (Cieply and Smejkal 2013). Blue dots indicate results obtained for a class of potentials including Gaussian, exponential, and Hulthen Liverts and Barnea (2011). Red dots at the edge of the allowed parameter region present predictions of very narrow and weakly bound states of ^{4}He-η, with binding energies and widths in the range of ~2–230 keV and ~8–64 keV. respectively, that are found by solving the Klein Gordon equation as in Ikeno et al. (2017). These states correspond to the optical potential parameters $|V_0|$ in the range from 58 to 65 MeV and $W_0 = 0.5$ MeV.

The η' -Nucleus Interaction and the Search for η' Mesic States

The η' -Nucleus Potential

Determination of the η'-Proton Scattering Length

Information on the η'-proton scattering length has been obtained from studies of the $\mathrm{pp} \rightarrow \mathrm{pp}\eta'$ reaction near threshold at COSY (Moskal et al. 2000; Czerwinski et al. 2014). The first measurement showed that the η'-p scattering length is of the order of 0.1 fm. In the second measurement, the reaction was studied with high statistics up to an excess energy of 11 MeV above threshold, where the cross section is clearly s-wave dominated. Fitting the excitation function, an analysis of the η' final state interaction in η' production in proton-proton collisions yields an η'-nucleon scattering length in free space of

$$a_{\eta'\mathrm{p}} = (0 \pm 0.43) + i(0.37\ ^{+0.40}_{-0.16})\ \mathrm{fm}, \tag{12}$$

indicating a relatively weak η' nucleon interaction (Czerwinski et al. 2014). Using Eqs. (1,2,3), the real and imaginary part of the η'-p scattering length can be converted into the real and imaginary part of the η'-nucleus potential

$$U_0 = V_0 + i \cdot W_0 = -(0 \pm 37.9 + i \cdot 32.6\,^{+35.2}_{-14.1})\ \text{MeV} \tag{13}$$

for comparison to direct determinations of the η'-nucleus potential parameters in the following sections.

Analyzing polarization observables and differential cross sections measured in the $\gamma p \to p\eta'$ reaction (Levi Sandri et al. 2015; Collins et al. 2017; Kashevarov et al. 2017), Anisovich et al. (2018) obtain within a coupled channels model a modulus of the $\eta' p$ scattering length of

$$|a_{\eta' N}| = 0.403 \pm 0.015 \pm 0.060\ \text{fm} \tag{14}$$

The phase has been determined to be $87° \pm 2°$ which implies a small real part and sizable absorption, consistent with the result of Czerwinski et al. (2014) but in conflict with the data on η' photoproduction off nuclei discussed below. A purely imaginary η' scattering length is however not expected as discussed in the section "Modeling the η' and η in Medium". Independent experiments and analyses are needed to clarify this point.

Determination of the Imaginary Part of the η'-Nucleus Potential From Measurements of the Transparency Ratio

The imaginary part $W(r)$ of the complex meson-nucleus potential $U(r) = V(r) + iW(r)$ is a measure for the absorption of the meson in the nuclear medium. Hereby, r is the distance from the center of the nucleus which serves as a production target for the short-lived meson as well as an absorber. The reduction of the meson flux in the nuclear target can be quantified by the transparency ratio defined as (Hernandez and Oset 1992; Cabrera et al. 2004)

$$T_A = \frac{\sigma_A}{A \cdot \sigma_N} \tag{15}$$

which compares the meson production cross section off the nucleus with mass number A to A times the production cross section off the free nucleon. Thus, in case of no absorption, $T_A = 1$, if secondary production processes can be neglected. Experimentally, the transparency ratio T_A is determined by measuring the meson production cross section off the nucleus with mass number A and relating it to the production cross section off the proton or a light nucleus like ^{12}C.

The absorption of the meson shortens its lifetime in the nuclear medium and therefore increases its width $\Gamma(\rho_N)$. For a linear density dependence, the width $\Gamma(\rho_N)$ at nuclear density ρ_N is given by

$$\Gamma(\rho_N) = \Gamma_0 \cdot (\rho_N(r)/\rho_0) \tag{16}$$

where Γ_0 is the width at normal nuclear density ρ_0 . The imaginary potential $W(r)$ is then related to the in-medium width Γ_0 via

$$W(r) = -\frac{1}{2} \cdot \Gamma_0 \cdot \frac{\rho_N(r)}{\rho_0} \tag{17}$$

As described in Metag et al. (2017), Nanova et al. (2012), and Friedrich et al. (2016), the transparency ratio can be calculated with Glauber-, transport- or collisional-model approaches for any in-medium width Γ_0. Conversely, comparing the measured transparency ratio to the model results, the in-medium width Γ_0 and thus by Eq. (17) the imaginary part of the meson-nucleus potential can be deduced.

The result of the first measurement of the η' transparency ratio in the $\gamma A \rightarrow \eta' + X$ reaction for Ca, Nb, and Pb is shown in Fig. 8 (left). A comparison of the experimental results with transport calculations leads to an in-medium width at normal nuclear density of about 20 MeV (Nanova et al. 2012).

For the existence and observability of meson-nucleus bound states, the in-medium width near the production threshold, i.e., at low meson momenta relative to the nuclear environment, is decisive. For extrapolating to low momenta, the transparency ratio has to be measured over a broad momentum or energy range. As an example, Fig. 8 (right) (Friedrich et al. 2016) shows the imaginary potential for η' mesons in Nb as function of the excess energy above threshold, derived from a Glauber model analysis of transparency ratio measurements for each excess energy bin. The extrapolation to the production threshold using different fit functions yields an imaginary part of the η'-Nb potential at normal nuclear matter density of $W(\rho_0) = (13 \pm 3(\text{stat.}) \pm 3(\text{syst.}))$ MeV, consistent with the earlier result (Nanova et al. 2012). Further details of this extraction and a discussion of uncertainties can

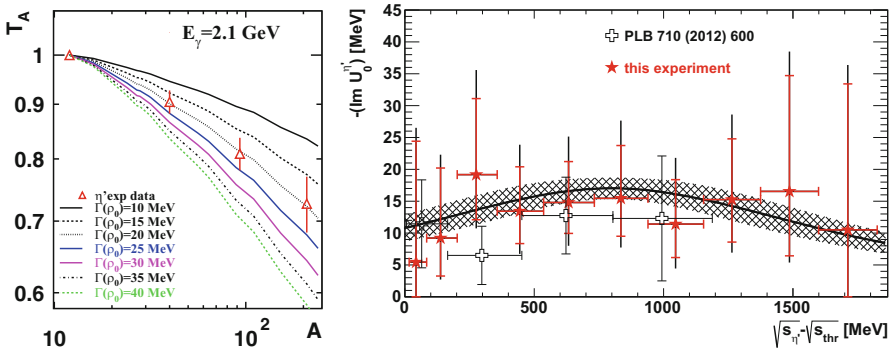

Fig. 8 (Left): η' transparency ratio for Ca, Nb, and Pb normalized to that for C as function of the nuclear mass number in comparison to transport model calculations for different in-medium widths Γ_0 (Nanova et al. 2012). (Right): Imaginary part of the η'-Nb potential as function of the available energy (red stars) (Friedrich et al. 2016) in comparison to earlier measurements (open crosses) (Nanova et al. 2012). The solid curve is a fit to the data with a Breit-Wigner function. The shaded area indicates a confidence level of $\pm 1\sigma$ of the fit curve, taking statistical and systematic errors into account. (The figures are taken from Nanova et al. (2012) and Friedrich et al. (2016), respectively. With kind permission of The European Physical Journal (EPJ))

be found in the original literature Friedrich et al. (2016) or the review Metag et al. (2017).

Determination of the Real Part of the η' Nucleus Potential by Measuring Excitation Functions and/or Momentum Distributions

A measurement of the meson production cross section as a function of the incident beam energy is sensitive to in-medium modifications of the meson since a downward mass shift would lower the production threshold and thus increase the production cross section at a given incident beam energy due to the enlarged phase-space. Furthermore, transport calculations (Weil et al. 2013) have demonstrated that also the momentum distribution of mesons produced off nuclei is sensitive to the in-medium properties of the meson. When leaving the nucleus, a meson with reduced in-medium mass has to get back to its free vacuum mass. The missing mass has to be generated at the expense of its kinetic energy. Consequently, this energy-to-mass conversion shifts the meson momentum distribution to lower average values.

The measurement of the η' excitation function and momentum distribution have both been used to extract the in-medium mass shift of the η' meson in Nb as shown in Fig. 9. An enhancement of the total cross section and a shift towards lower momenta compared to a scenario without mass modification is observed. A quantitative comparison with collision model calculations yields in-medium mass shifts of $-(40\pm12)$ MeV and $-(45\pm20)$ MeV, respectively. Further inclusive measurements have been performed on carbon (Nanova et al. 2013) as well as a semi-inclusive study of low momentum η' mesons in coincidence with high energy forward going protons which take over most of the momentum of the incident beam (Nanova et al. 2018). The values extracted for the real part of the η'-nucleus potential do not show a significant mass dependence and are summarized in Fig. 10 (Nanova et al. 2018).

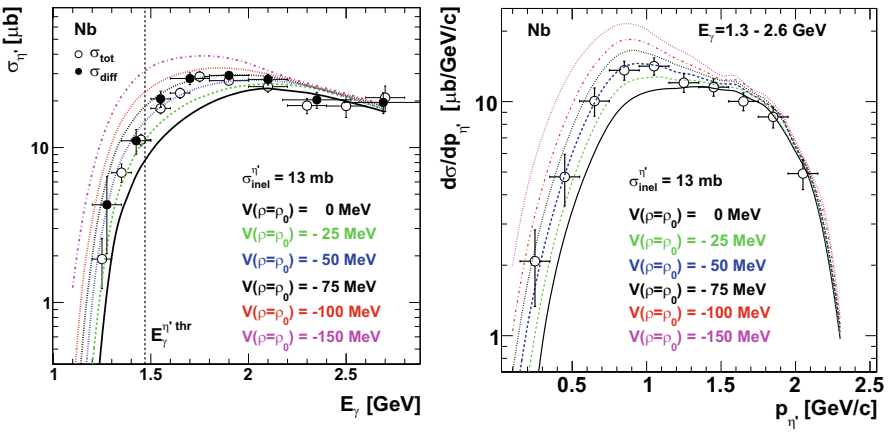

Fig. 9 Excitation function (left) and momentum distribution (right) of η' mesons produced in the reaction $\gamma p \rightarrow \eta' X$ in comparison to collision model calculations for different values of the real part of the η'-Nb potential. (The figures are taken from Nanova et al. 2016)

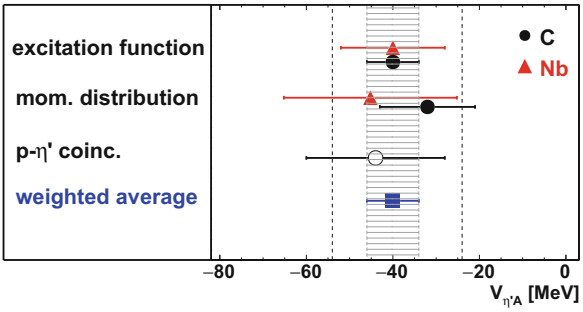

Fig. 10 Depth of the real part of the η'-nucleus potential derived from inclusive measurements on C (Nanova et al. 2013) and Nb (Nanova et al. 2016) and from an η'-p coincidence experiment (Nanova et al. 2018). The weighted overall average is represented by a blue box. The shaded area indicates the statistical error. The dashed lines mark the range of systematic uncertainties. (The figure is taken from Nanova et al. (2018). With kind permission of The European Physical Journal (EPJ))

Parameters of the η'-Nucleus Potential

As described in the preceding sections, the parameters of the η'-nucleus potential have not been directly measured but have been extracted from experimental observables such as transparency ratios, excitation functions, and meson momentum distributions using transport and collision models and Glauber calculations. Only models that have been widely tested and successfully applied in other areas of nuclear and hadron physics have been used, giving consistent results in the present analysis. The experimental results have been reproduced in a long series of independent experiments over several years. In view of these consistencies, the following final values of the real and imaginary part of the η'-nucleus potential are quoted:

$$V(\rho = \rho_0) = -(40 \pm 6(\text{stat}) \pm 15(\text{syst}))\text{MeV} \tag{18}$$

$$W(\rho = \rho_0) = -(13 \pm 3(\text{stat}) \pm 3(\text{syst}))\,\text{MeV} \tag{19}$$

Theoretical predictions for the real part of the η-nucleus potential cover a broad range from -150 MeV (Nagahiro et al. 2006), -80 MeV (Sakai and Jido 2013), -40 MeV (Bass and Thomas 2006) to 0 MeV (Bernard and Meißner 1988). Only the result of Bass and Thomas (2006) is close to the experimental value. A more detailed discussion of the experimental uncertainties and the comparison to theory is given in Metag et al. (2017).

More direct information on the η'-nucleus potential will be accessible from the observation of η'-nucleus bound states. As the modulus of the real part of the potential is found to be about 3 times larger than the modulus of the imaginary

part – a favorable condition for the observation of meson-nucleus bound states – the η' meson appears to be a promising candidate in the search of mesic states.

Direct Searches for η' Mesic States

Search for η'-Mesic States in the ^{12}C(p, d)^{11}C $\otimes$ η' Reaction

The first pioneering experiment searching for η' bound states was performed in 2014 at the Fragment Separator (FRS) at GSI using the ^{12}C(p,d) reaction (Tanaka et al. 2016, 2018). The incident proton energy of 2.5 GeV was chosen to achieve almost recoil-less production of the η' meson. A deuteron with high momentum is ejected to forward angles, while the η' meson produced with low momentum could be bound to the ^{11}C. In the experiment, only the deuteron momentum distribution has been measured, applying missing mass spectrometry.

In Fig. 11 (Left), the measured excitation spectrum of the ^{12}C(p,d) reaction near the η' emission threshold is shown (Tanaka et al. 2016). Because of the multi-pion background, no narrow structure has been observed in spite of the

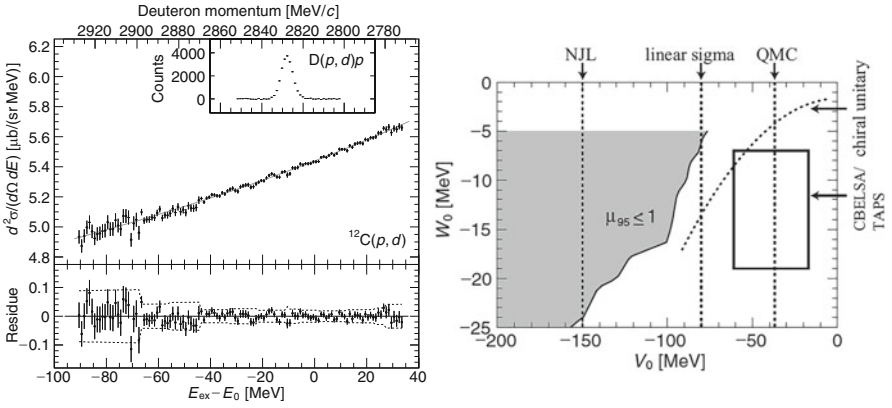

Fig. 11 (Left): Excitation energy spectrum of ^{11}C measured in the ^{12}C(p,d) reaction at a proton energy of 2.5 GeV. The abscissa represents the excitation relative to the η' production threshold E_0 = 957.78 MeV. The gray curve is a third-order polynomial fit to the data. The inset shows the momentum spectrum measured in the elastic D(p,d)p reaction. (Bottom panel): Fit residues with 2σ envelopes. (Right): the imaginary part versus the real part of the η'-nucleus potential. The shaded area above the solid curve indicates the parameter range which is excluded by the FRS measurement (Tanaka et al. 2016, 2018). Summing systematic and statistical errors, the box represents the range of V_0 and W_0 parameters determined by the CBELSA/TAPS collaboration (Nanova et al. 2013, 2016; Friedrich et al. 2016; Nanova et al. 2018) (see section "The η' -Nucleus Potential"). Theoretical predictions with the NJL model (Nagahiro et al. 2006), the linear sigma model (Sakai and Jido 2013), the QMC model (Bass and Thomas 2006), and the chiral unitary approach (Nagahiro et al. 2012) are shown by dashed lines. (The figures are taken from Tanaka et al. 2016, 2018, respectively)

extremely good statistical sensitivity. An upper limit for the formation cross section of η'-mesic nuclei of ≈20 nb/(sr MeV) near the threshold has been deduced. In a detailed analysis, the experimental spectrum has been compared to theoretical predictions (Nagahiro et al. 2013) for different potential parameters (V_0, W_0), allowing an exclusion of certain parameter ranges as indicated in Fig. 11 (right). A strongly attractive potential of $V_0 \approx -150$ MeV predicted by the NJL model calculations (Nagahiro et al. 2013) can be rejected. Other sets of predicted potential parameters, also shown in Fig. 11 (right), cannot be excluded. The experimental result is consistent with the potential parameters determined in the photoproduction experiments discussed in the section "The η' -Nucleus Potential".

An improved follow-up experiment (Itahashi et al.) has been performed providing higher sensitivity by combining missing mass spectrometry with simultaneous detection of protons from the decay of the η'-mesic states. An important decay mode is two-nucleon absorption $\eta'\mathrm{NN} \rightarrow \mathrm{NN}$ yielding protons with 300–600 MeV in the laboratory. Simulations have shown that by selecting energetic protons in the backward angular range the multi-pion background can be efficiently suppressed. In comparison to the pioneering experiment, the signal-to-background ratio will be improved by two orders of magnitude. The results are eagerly awaited.

Search for η'-Mesic States in the ^{12}C(γ, p) Reaction

The idea of combining missing mass spectrometry with coincident detection of decay products of the η'-mesic state has already been realized in the experiment by the LEPS2/BGOegg collaboration at Spring-8 (Tomida et al. 2020).

Using photon beams of 1.3–2.4 GeV generated by laser backscattering, the following reaction has been studied in small momentum transfer kinematics:

$$\gamma + {}^{12}\mathrm{C} \rightarrow \mathrm{p}_f + \eta' \otimes {}^{11}\mathrm{B} \tag{20}$$

in coincidence with η-proton pairs from

$$\eta' + \mathrm{p} \rightarrow \eta + \mathrm{p}_s \tag{21}$$

which is expected to be the strongest absorption process for an η' meson bound to a nucleus. The forward going proton p_f is used for missing mass spectrometry, while the sideward going proton p_s together with the η meson tags the decay of the η' mesic state. Since the bound η' meson is almost at rest, the η and proton will be emitted nearly back-to-back in the laboratory. By the simultaneous measurement of the (η, p_s) pair and the forward going proton p_f, the multi-pion background can be effectively suppressed.

As shown in Fig. 12, no signal events have, however, been observed in the bound state region leading to an upper limit of the signal cross section of 2.2 nb/sr at the 90% confidence level for opening angles $\cos\theta_{\mathrm{lab}}^{\mathrm{p}\eta} \geq -0.9$. An attempt has been made to extract from this result an upper limit for the formation cross section of an $\eta' \otimes {}^{11}$B state with subsequent ($\eta + \mathrm{p}_s$) decay. By comparing to a theoretical cross section (Nagahiro 2017), the real part V_0 of the $\eta' - {}^{11}$B optical potential and

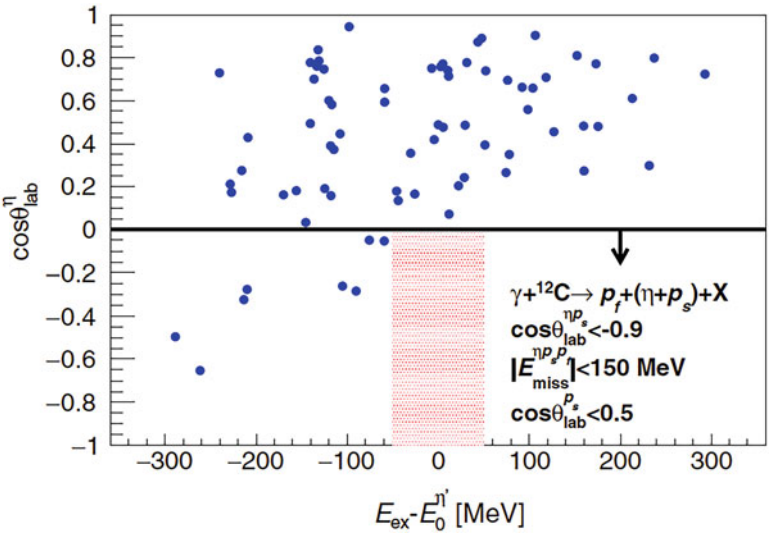

Fig. 12 Two-dimensional plot of $\cos\theta^{\eta}_{\rm lab}$ vs. $E_{ex} - E_0^{\eta'}$ for the $(\eta + \mathrm{p}_s)$, p_f coincidence data. The expected signal region is marked by red hatching. (The figure is taken from Tomida et al. (2020). With kind permission of the American Physical Society)

the branching fraction $\mathrm{BR}_{\eta'\mathrm{N}\to\eta\mathrm{N}}$ for the decay via the $(\eta + \mathrm{p}_s)$ channel have been constrained. Hereby, the theoretical cross section has been normalized to reproduce the measured η' cross section in the unbound region near the production threshold. Tomida et al. (2020) deduce an upper limit for the branching ratio $\mathrm{BR}_{\eta'\mathrm{N}\to\eta\mathrm{N}}$ of 24% for a potential depth $V_0 = -100$ MeV and of 80% for $V_0 = -20$ MeV, respectively, at the 90% confidence level. They conclude that $\mathrm{BR}_{\eta'\mathrm{N}\to\eta\mathrm{N}}$ is small and/or the real part V_0 of the η'-nucleus potential is shallow. However, in a comment to this work, Fujioka et al. (2021) point out several uncertainties in this analysis and claim that V_0 and $\mathrm{BR}_{\eta'\mathrm{N}\to\eta\mathrm{N}}$ may be over constrained.

Conclusions

In spite of numerous experimental efforts, η- and η'-nucleus bound states have so far not been directly observed. However, information on the strength of the η and η' interaction with nuclei has been deduced. A strong η-nucleus interaction has been experimentally established in hadron- and photon-induced reactions independent of the entrance channel dynamics. Comparing model calculations with cross section measurements as a function of the excitation energy, parameters of the real and imaginary part of the optical potential have been constrained to $V_0 = -60$ to 0 MeV and $W_0 = -5$ to 0 MeV in the case of ^{4}He. For the η' meson, the corresponding potential parameters are in the range of $V_0 \approx -40$ MeV and $W_0 \approx -13$ MeV. Both

parameter sets indicate an attractive meson-nucleus interaction and a relatively weak meson absorption.

On the theoretical side, interest is in understanding the role of gluonic degrees of freedom in the QCD phase diagram and (partial) restoration of axial U(1) symmetry at finite nuclear density. What makes the η' and η special compared to other mesons not sensitive to the gluonic potential that gives the η' and η extra mass? Future work might focus on extending model treatments of the η' and η in medium to make closer, more direct, connection with QCD and the symmetries of anomalous Ward identities at finite density as well as at finite temperature.

The search for η, η' mesic states continues. Promising results on the possible existence of a (virtual) η-d state have recently been presented by the ELPH group and need further independent confirmation. The coherent $\pi^0\eta$ photoproduction off nuclei appears to be a promising approach for further searches of η-nucleus bound states. Selecting events with a high π^0-momentum will render η-mesons with a small momentum relative to the intact nucleus, allowing for an enhanced formation of a bound state. Measuring simultaneously the production and decay of the mesic state, the approach pioneered by the Spring 8 experiment and the WASA@FRS measurement will hopefully reach the required sensitivity for the observation of an η'-nucleus bound state. The sensitivity of the Spring 8 experiment will be increased by studying a variety of other potential decay modes of the η'-nucleus bound states. New results are expected in the coming years.

Acknowledgments P.M. acknowledges the support from the Polish National Science Center through grant No. 2016/23/B/ST2/00784 and the EU Horizon 2020 research and innovation program, STRONG-2020 project, under grant agreement No 824093.

References

H.-H. Adam et al., arXiv:nucl-ex/0411038 (2004)
H.H. Adam et al. [COSY-11 Collaboration], Phys. Rev. C **75**, 014004 (2007)
P. Adlarson et al. [WASA-at-COSY Collaboration], Phys. Rev. C **88**, 055208 (2013)
P. Adlarson et al. [WASA-at-COSY Collaboration], Eur. Phys. J. A **50**, 100 (2014)
P. Adlarson et al. [WASA-at-COSY Collaboration], Nucl. Phys. A **959**, 102 (2017)
P. Adlarson et al. [WASA-at-COSY Collaboration], Phys. Lett. B **782**, 297 (2018)
P. Adlarson et al. [WASA-at-COSY Collaboration], Phys. Lett. B **802**, 135205 (2020a)
P. Adlarson et al. [WASA-at-COSY Collaboration], Phys. Rev. C **102**, 044322 (2020b)
S.V. Afanasiev et al., Phys. Part. Nucl. Lett. **8**, 1073 (2011)
C.A. Aidala, S.D. Bass, D. Hasch, G.K. Mallot, Rev. Mod. Phys. **85**, 655 (2013)
F. Ambrosino et al., JHEP **0907**, 105 (2009)
A.V. Anisovich et al., Phys. Lett. B **785**, 626 (2018)
S. Aoki et al. [JLQCD], Phys. Rev. D **103**, 074506 (2021)
R.A. Arndt et al., Phys. Rev. C **72**, 045202 (2005)
J.J. Aubert et al. [European Muon Collaboration], Phys. Lett. **123B**, 275 (1983)
R. Averbeck et al. [TAPS Collaboration], Z. Phys. A **359**, 65 (1997)
P. Ball, J.M. Frere, M. Tytgat, Phys. Lett. B **365**, 367 (1996)
N. Barnea, B. Bazak, E. Friedman, A. Gal, Phys. Lett. B **771**, 297 (2017a). Erratum: [Phys. Lett. B **775**, 364 (2017)]

N. Barnea, E. Friedman, A. Gal, Nucl. Phys. A **968**, 35 (2017b)
R. Barth et al. [KaoS Collaboration], Phys. Rev. Lett. **78**, 4007 (1997)
V.A. Baskov et al., Proc. Sci. Baldin-ISHEPP-XXI, 102 (2012)
S.D. Bass, Phys. Lett. B **463**, 286 (1999)
S.D. Bass, Rev. Mod. Phys. **77**, 1257 (2005)
S.D. Bass, Acta Phys. Polon. B **52**, 43 (2021)
S.D. Bass, E. Marco, Phys. Rev. D **65**, 057503 (2002)
S.D. Bass, P. Moskal, Rev. Mod. Phys. **91**, 015003 (2019)
S.D. Bass, A.W. Thomas, Phys. Lett. B **634**, 368 (2006)
S.D. Bass, A.W. Thomas, Acta Phys. Polon. B **41**, 2239 (2010)
S.D. Bass, A.W. Thomas, Acta Phys. Polon. B **45**, 627 (2014)
A. Bazavov et al. [HotQCD Collaboration], Phys. Rev. D **86**, 094503 (2012)
J. Berger et al. [SPES4 Collaboration], Phys. Rev. Lett. **61**, 919 (1988)
V. Bernard, U.-G. Meißner, Phys. Rev. D **38**, 1551 (1988)
M. Betigeri et al. [GEM Collaboration], Phys. Lett. B **472**, 267 (2000)
R.S. Bhalerao, L.C. Liu, Phys. Rev. Lett. **54**, 865 (1985)
R. Bilger et al. [WASA/PROMICE Collaboration], Phys. Rev. C **65**, 044608 (2002)
J.D. Bjorken, Phys. Rev. **148**, 1467 (1966)
J.D. Bjorken, Phys. Rev. D **1**, 1376 (1970)
P. Braun-Munzinger, J. Wambach, Rev. Mod. Phys. **81**, 1031 (2009)
A. Budzanowski et al. [GEM Collaboration], Nucl. Phys. A **821**, 193 (2009a)
A. Budzanowski et al. [GEM Collaboration], Phys. Rev. C **79**, 012201 (2009b)
D. Cabrera et al., Nucl. Phys. A **733**, 130 (2004)
R.E. Chrien et al., Phys. Rev. Lett. **60**, 2595 (1988)
K. Cichy et al. [ETM], JHEP **09**, 020 (2015)
A. Cieply, J. Smejkal, Nucl. Phys. A **919**, 46 (2013)
A. Cieplý, E. Friedman, A. Gal, J. Mareš, Nucl. Phys. A **925**, 126 (2014)
I.C. Cloet, W. Bentz, A.W. Thomas, Phys. Rev. Lett. **95**, 052302 (2005)
I.C. Cloët et al., J. Phys. G **46**(9), 093001 (2019)
R. Collins et al. [CLAS Collaboration], Phys. Lett. B **771**, 213 (2017)
E. Czerwinski et al., Phys. Rev. Lett. **113**, 062004 (2014)
L. de Barbaro, K.J. Heller, J. Szwed, Jagiellonian University preprint TPJU-24/84 (1984)
T.A. DeGrand, R.L. Jaffe, K. Johnson, J.E. Kiskis, Phys. Rev. D **12**, 2060 (1975)
P. Di Vecchia, G. Veneziano, Nucl. Phys. B **171**, 253 (1980)
S.D. Drell, A.C. Hearn, Phys. Rev. Lett. **16**, 908 (1966)
M. Ericson, Acta Phys. Polon. B **29**, 2349–2356 (1998)
T.E.O. Ericson, W. Weise, *Pions and Nuclei*. International Series of Monographs on Physics, vol. 74 (Oxford University Press, Oxford 1988)
M. Ericson, A. Figureau, C. Thevenet, Phys. Lett. B **45**, 19–22 (1973)
T. Feldmann, P. Kroll, B. Stech, Phys. Lett. B **449**, 339 (1999)
A. Fix, O. Kolesnikov, Phys. Lett. B **772**, 663 (2017)
R. Frascaria et al. [SPES4 Collaboration], Phys. Rev. C **50**, R537 (1994)
E. Friedman, A. Gal, Phys. Rep. **452**, 89 (2007)
E. Friedman, A. Gal, J. Mareš, Phys. Lett. B **725**, 334 (2013)
S. Friedrich et al., Eur. Phys. J. A **52**(9), 297 (2016)
H. Fujioka et al., Phys. Rev. Lett. **126**, 019201 (2021)
C. Garcia-Recio, J. Nieves, T. Inoue, E. Oset, Phys. Lett. B **550**, 47 (2002)
J. Gasser, H. Leutwyler, Phys. Rep. **87**, 77 (1982)
M. Gell-Mann, R.J. Oakes, B. Renner, Phys. Rev. **175**, 2195 (1968)
S.B. Gerasimov, Sov. J. Nucl. Phys. **2**, 430 (1966) [Yad. Fiz. **2**, 598 (1965)]
F.J. Gilman, R. Kauffman, Phys. Rev. D **36**, 2761 (1987); Erratum [Phys. Rev. D **37**, 3348 (1988)]
P. Goslawski et al., Prog. Part. Nucl. Phys. **67**, 370 (2012)
A.M. Green, S. Wycech, Phys. Rev. C **55**, R2167 (1997)
A.M. Green, S. Wycech, Phys. Rev. C **71**, 014001 (2005)

E. Gregory et al., JHEP **1210**, 170 (2012)
P.A.M. Guichon, Phys. Lett. B **200**, 235 (1988)
P.A.M. Guichon, K. Saito, E.N. Rodionov, A.W. Thomas, Nucl. Phys. A **601**, 349 (1996)
V. Guzey, M. Strikman, Phys. Rev. C **61**, 014002 (2000)
Q. Haider, L.C. Liu, Phys. Lett. B **172**, 257 (1986)
E. Hernandez, E. Oset, Z. Phys. A **341**, 201 (1992)
N. Ikeno et al., Eur. Phys. J. A **53**, 194 (2017)
T. Ishikawa et al., Phys . Rev. C **104**, L052201 (2021)
K. Itahashi et al., accepted proposal GSI-S547 (2020)
J.I. Kapusta, D. Kharzeev, L.D. McLerran, Phys. Rev. D **53**, 5028 (1996)
V.L. Kashevarov et al., Phys. Rev. Lett. **118**, 247 (2017)
N.G. Kelkar, Eur. Phys. J. A **52**, 309 (2016)
N.G. Kelkar, H. Kamada, M. Skurzok, Int. J. Mod. Phys. E **28**, 1950066 (2019)
N.G. Kelkar, D. Bedoya Fierro, H. Kamada, M. Skurzok, Nucl. Phys. A **996**, 121698 (2020)
P. Kienle, T. Yamazaki, Prog. Part. Nucl. Phys. **52**, 85 (2004)
H. Lenske, M. Dhar, Lect. Notes Phys. **948**, 161 (2018)
H. Lenske, M. Dhar, T. Gaitanos, X. Cao, Prog. Part. Nucl. Phys. **98**, 119 (2018)
H. Leutwyler, Nucl. Phys. Proc. Suppl. **64**, 223 (1998)
H. Leutwyler, Mod. Phys. Lett. A **28**, 1360014 (2013)
R. Levi Sandri et al., Eur. Phys. J. A **51**, 77 (2015)
Y.R. Liu, S.L. Zhu, Phys. Rev. D **75**, 034003 (2007)
E.Z. Liverts, N. Barnea, J. Phys. A **44**, 375303 (2011)
B. Mayer et al. [SPES2 Collaboration], Phys. Rev. C **53**, 2068 (1996)
L. McLerran, Acta Phys. Polon. B **51**, 1067 (2020)
T. Mersmann et al. [ANKE Collaboration], Phys. Rev. Lett. **98**, 242301 (2007)
V. Metag, M. Nanova, E.Y. Paryev, Prog. Part. Nucl. Phys. **97**, 199 (2017)
C.J. Morningstar, M.J. Peardon, Phys. Rev. D **60**, 034509 (1999)
P. Moskal, J. Smyrski, Acta Phys. Pol. B **41**, 2281 (2010)
P. Moskal et al., Phys. Lett. B **482**, 356 (2000)
H. Nagahiro, JPS Conf. Proc. **13**, 010010 (2017)
H. Nagahiro, M. Takizawa, S. Hirenzaki, Phys. Rev. C **74**, 045203 (2006)
H. Nagahiro, S. Hirenzaki, E. Oset, A. Ramos, Phys. Lett. B **709**, 87 (2012)
H. Nagahiro et al., Phys. Rev. C **87**, 045201 (2013)
M. Nanova et al. [CBELSA/TAPS Collaboration], Phys. Lett. B **710**, 600 (2012)
M. Nanova et al. [CBELSA/TAPS Collaboration], Phys. Lett. B **727**, 417 (2013)
M. Nanova et al. [CBELSA/TAPS Collaboration], Phys. Rev. C **94**, 025205 (2016)
M. Nanova et al., Eur. Phys. J. A **54**, 182 (2018)
E. Oset, L.L. Salcedo, Nucl. Phys. A **468**, 631 (1987)
M. Papenbrock et al. [ANKE Collaboration], Phys. Lett. B **734**, 333 (2014)
M. Pfeiffer et al., Phys. Rev. Lett. **92**, 252001 (2004)
F. Pheron et al., Phys. Lett. B **709**, 21 (2012)
T. Rausmann et al. [ANKE Collaboration], Phys. Rev. C **80**, 017001 (2009)
M. Röbig-Landau et al., Phys. Lett. B **373**, 45 (1996)
K. Saito, K. Tsushima, A.W. Thomas, Prog. Part. Nucl. Phys. **58**, 1–167 (2007)
S. Sakai, D. Jido, Phys. Rev. C **88**, 064906 (2013)
A. Schroter et al., Z. Phys. A **350**, 101 (1994)
H. Shimizu [BGOegg Collaboration], Acta Phys. Polon. B **48**, 1819 (2017)
G.M. Shore, Lect. Notes Phys. **737**, 235 (2008)
G.M. Shore, G. Veneziano, Nucl. Phys. B **381**, 23 (1992)
A. Sibirtsev et al., nal state interaction in incoherent photoproduction of mesons from the deuteron near threshold Phys. Rev. C **65**, 044007 (2002)
M. Skurzok, Few-Body Syst. **62**, 5 (2021)
M. Skurzok et al., Phys. Lett. B **782**, 6 (2018)
M. Skurzok et al., Nucl. Phys. A **993**, 121647 (2020)

J. Smyrski et al. [COSY-11 Collaboration], Phys. Lett. B **649**, 258 (2007)
A. Sobczyk, J. Szwed, Acta Phys. Polon. B **32**, 2947 (2001)
J. Suhonen, Acta Phys. Polon. B **49**, 237 (2018)
K. Suzuki et al., Phys. Rev. Lett. **92**, 072302 (2004)
Y.K. Tanaka et al. [Eta-PRiME/Super-FRS Collaboration], Phys. Rev. Lett. **117**, 202501 (2016)
Y.K. Tanaka et al. [Eta-PRiME/Super-FRS Collaboration], Phys. Rev. C **97**, 015202 (2018)
H. Toki, S. Hirenzaki, T. Yamazaki, R.S. Hayano, Nucl. Phys. A **501**, 653 (1989)
N. Tomida et al., Phys. Rev. Lett. **124**, 202501 (2020)
A. Tomiya et al., Phys. Rev. D **96**, 034509 (2017); Addendum [Phys. Rev. D **96**, 079902 (2017)]
K. Tsushima, Nucl. Phys. A **670**, 198 (2000)
K. Tsushima, D.H. Lu, A.W. Thomas, K. Saito, Phys. Lett. B **443**, 26 (1998)
G. Veneziano, Nucl. Phys. B **159**, 213 (1979)
J. Weil, U. Mosel, V. Metag, Phys. Lett. B **723**, 120 (2013)
C. Wilkin et al. [ANKE Collaboration], Phys. Lett. B **654**, 92 (2007)
N. Willis et al. [SPES3 Collaboration], Phys. Lett. B **406**, 14 (1997)
E. Witten, Nucl. Phys. B **156**, 269 (1979)
E. Witten, Ann. Phys. **128**, 363 (1980)
A. Wronska et al. [ANKE Collaboration], Eur. Phys. J. A **26**, 421 (2005)
S. Wycech, W. Krzemien, Acta Phys. Polon. B **45**, 745 (2014)
T. Yamazaki et al., Z. Phys. A **355**, 219 (1996)
T. Yorita et al., Phys. Lett. B **476**, 226 (2000)
P.A. Zyla et al. [Particle Data Group], PTEP **2020**, 083C01 (2020)